Langmuir

Article

pubs.acs.org/Langmuir

MoS_2 Nanocrystals Confined in a DNA Matrix Exhibiting Energy Transfer

Nirmal Goswami, Anupam Giri, and Samir Kumar Pal*

Department of Chemical, Biological, and Macromolecular Sciences, S. N. Bose National Centre for Basic Sciences, Block JD, Sector III, Salt Lake, Kolkata 700 098, India

Supporting Information

ABSTRACT: We report the wet chemical synthesis of MoS_2 nanocrystals (NCs), a transition-metal dichalcogenide, using DNA as a host matrix. As evidenced from transmission electron microscopy (TEM), the NCs are highly crystalline, with an average diameter of ~5 nm. Ultraviolet−visible (UV−vis) absorption studies along with band gap calculations confirm that NCs are in quantum confinement. A prominent red shift of the optical absorption bands has been observed upon formation of the thin film using hexadecyltrimethylammonium chloride (CTAC), i.e., in the case of MoS_2@DNA−CTAC. In the thin film, strong electron−phonon coupling arises because of the resonance effect, which is reflected from the emergence of intense first-, second-, and third-order Raman peaks, whenever excited with the 488 nm line. We have established that our as-synthesized MoS_2 NCs quench the fluorescence of a well-known DNA minor groove binding probe, Hoechst 33258. Unprecedented fluorescence quenching (94%) of donor (Hoechst 33258) emission and efficient energy transfer (89%) between Hoechst 33258 and MoS_2 NCs (acceptor) are obtained. The donor−acceptor distance of these conjugates has been described by a Förster resonance energy transfer (FRET)-based model. Furthermore, employing a statistical method, we have estimated the probability of the distance distribution between the donor and acceptor. We believe that the study described herein may enable substantial advances in fields of optoelectronics, photovoltaics, catalysis, and many others.

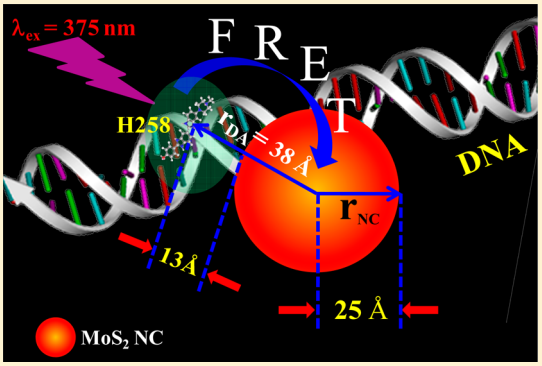

INTRODUCTION

Transition-metal chalcogenide semiconductors display interesting properties that are important for sensing, catalysis, photovoltaics, and even biology.[1−8] In particular, molybdenum disulfide (MoS_2) is a prototypical transition-metal dichalcogenide material, which consists of covalently bonded Mo and S atoms. It is an indirect band gap semiconductor in its bulk form, with a band gap of 1.29 eV.[9] These nanomaterials have been known in the form of layered two-dimensional (2D) sheet, nested fullerene-like nanodots, inorganic nanotubes, or even as nanocrystals (NCs).[10−14] Although graphene is the best among all of the known 2D materials, MoS_2 nanosheets have proven to be certainly promising because they exhibit robust mechanical properties and superior electrical performance.[15,16] MoS_2 is also an effective lubricant because of its layered structure. Ultrathin layers of MoS_2 display strong photoluminescence that increases when the material is thinned from multilayer to monolayer because of the indirect−direct transition, arising from quantum confinement effects.[17] Nanostructured MoS_2 has been demonstrated to be an efficient catalyst for hydrogen evolution reaction (HER) and hydrodesulfurization (HDS).[18] The fact that all of these intense properties are combined in one material implies that MoS_2 could also be one of the most valuable materials in nanotechnology.

MoS_2 nanosheets, nanofibers, and nanorods have been prepared by a number of techniques, such as liquid exfoliation,[19] vapor deposition,[20] hydrothermal,[21] electrospinning,[22] wet chemical methods,[23] etc. At the same time, the colloidal synthesis of MoS_2 NCs is quite delicate, and as a result, there is less development compared to other synthetic routes. MoS_2 nanoparticles (NPs) having a size between 10 and 40 nm have been synthesized by the metal−organic chemical vapor deposition method.[24,25] Other approaches, such as sonochemical,[26] solvothermal,[27] or thermal decomposition methods,[28] do exist; however, the lack of size and shape control and produce poorly crystalline or totally amorphous products with little solvent dispersity. Yu et al. have reported less than 5 nm MoS_2 NCs, unfortunately dispersible only in organic solvents.[13] All of these methods involved complex or high-temperature reaction, and the morphology cannot be easily controlled. Therefore, it is still a challenge to develop a facile, room-temperature method to synthesize MoS_2 NCs.

The importance of finding a proper synthetic route for MoS_2 NCs has been a driving force for the present work. The use of biomolecules would be an interesting template for the synthesis of MoS_2 NCs because they are known to be nontoxic, viable,

Received: May 15, 2013
Published: August 9, 2013

 © 2013 American Chemical Society dx.doi.org/10.1021/la4028578 | Langmuir 2013, 29, 11471−11478

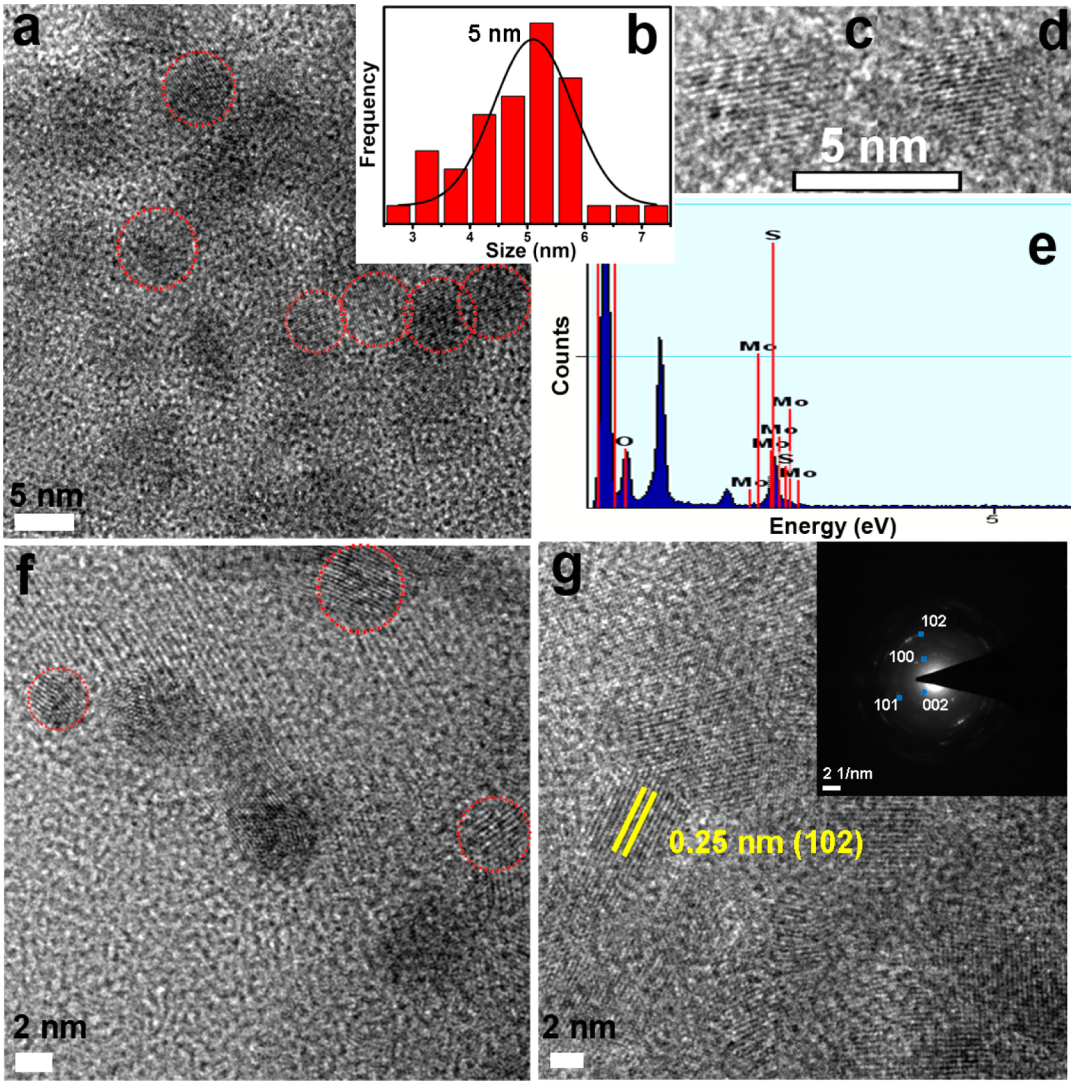

Figure 1. (a and f) TEM image of the MoS_2 NCs. (b) Size distribution curve. (c and d) HRTEM images of single MoS_2 NC. (e) EDAX spectrum collected for MoS_2@DNA. (g) HRTEM image and SAED pattern (inset).

and excellent protecting agents. Quantum dots of ZnS, CdS, HgS, and PbS have been synthesized using various biomolecules.[2,29−32] Among many biological systems that could participate in biomineralization and be indeed used as a biotemplate, DNA have been the subject of particular attention because of its excellent and predictable self-assembly properties, high rigidity of their double helices on the nanoscale, their stabilizing property, and most importantly, high affinity toward the metal cations. For example, self-assembled functionalization properties of DNA have enabled researchers to generate well-defined NPs, quantum dots, or even various superlattices.[31,33,34] Herein, we report a facile wet chemical synthesis of MoS_2 NCs using DNA macromolecules. To the best of our knowledge, this is the first time DNA has been used to synthesize and anchor MoS_2 NCs. A high-resolution transmission electron microscopy (HRTEM) study reveals that NPs are highly crystalline in nature, with an average diameter of ∼5 nm. Ultraviolet−visible (UV−vis) absorption study and the corresponding band gap calculation demonstrate that as-synthesized NCs are in quantum confinement compared to the bulk MoS_2. Moreover, our Raman spectroscopic studies indicate that the optically attractive MoS_2 NCs could be Raman-active in strong resonance conditions. The presence of a strong Raman peak at 447 cm^{-1} along with second- and third-order Raman lines in the case of the MoS_2 thin film further reinforces our justification on the resonance Raman effect. In the present study, we also establish that, akin to the other nanomaterials, MoS_2 NCs could be an efficient fluorescence quencher. For that, we have chosen Hoechst 33258 (referred to as H258 henceforth), which is well-known as a potential DNA minor groove binder. It could be a Förster resonance energy transfer (FRET) donor when confined in DNA. Afterward, we show efficient energy transfer between H258 and proximal MoS_2 NCs confined in DNA using steady-state and time-resolved spectroscopy. We first demonstrate a FRET-based model, which follows $1/r^6$ distance dependence, to calculate the donor−acceptor distance (r). We then explore the probability of donor−acceptor distance distribution using a simple mathematical model. Finally, employing the kinetic model developed by Tachiya (for the quenching of luminescent probes),[35,36] we analyze the picosecond-resolved fluorescence results to understand the kinetics of energy transfer.

dx.doi.org/10.1021/la4028578 | *Langmuir* 2013, 29, 11471−11478

EXPERIMENTAL SECTION

Salmon sperm DNA, sodium sulfide, sodium hydroxide, and $MoCl_5$ were obtained from Sigma-Aldrich. Hexadecyltrimethylammonium chloride (CTAC) and H258 were obtained from Invitrogen. Dimethylaniline, hydrazine, and hydrochloric acid (HCl) were from Merck. Millipore water was used throughout the experiments. All of the chemicals were used as received without further purification. The H258–DNA solution was prepared by adding a requisite amount of the probe in DNA solution and stirring for 1 h. The final concentration ratio of [DNA]/[H258] was 10:1.

Synthesis of MoS_2 NCs. It involves two steps. In the first step, an aqueous solution (5 mL) of DNA^-Na^+ from salmon testes (65 mg) and 5 mL of 100 mM $MoCl_5$ and H_2O were mixed at room temperature under vigorous stirring, with a final pH value of ~9 (adjusted by 1 M NaOH solution carefully). Then, the solution was allowed to stir for 6–8 h, so that the solution becomes colorless. In the second step, 5 mL of 200 mM Na_2S was added to 10 mL of as-synthesized Mo–DNA complexes, with a final pH value of ~6 (adjusted by HCl carefully), and the solution was stirred for 15 min. Completion of the reaction was observed visibly by color changes from colorless to yellow. Such a color transition is indicative of the formation of MoS_2 NCs.

Preparation of the MoS_2@DNA–CTAC Thin Film. An aqueous solution (5 mL) of as-prepared MoS_2@DNA (final DNA concentration was 6.5 mg/mL) was added to 5 mL of aqueous solution of CTAC (6.5 mg/mL). A 1:1 stoichiometric combination led to the spontaneous formation of the MoS_2@DNA–CTAC complex precipitate. The precipitate was collected by filtration, washed with distilled water, and then lyophilized for 48 h. Finally, a yellowish powder was obtained when dried in a vacuum at 37 °C. The powder was then dissolved in *n*-butanol; the solution was cast on a Teflon plate; and the solvent was evaporated slowly under the saturated vapor at room temperature. Finally, a yellowish, water-insoluble thin film was formed, which was used for spectroscopic characterization.

Instrumentation. *UV–vis Absorption Spectroscopy.* Optical absorption spectra of the solutions were measured with a Shimadzu spectrophotometer using a quartz cuvette of 1 cm path length.

Fluorescence Spectroscopy. Fluorescence spectra were recorded with Jobin Yvon Fluoromax-3 fluorimeter.

Circular Dichroism (CD) Spectroscopy. The CD spectra were measured in a Jasco 815 spectropolarimeter. The cell path length was 10 mm.

Fourier Transform Infrared (FTIR) Spectroscopy. A JASCO FTIR-6300 spectrometer was used to confirm the covalent attachment of the DNA with the MoS_2 NCs. For FTIR measurements, powdered samples were mixed with KBr powder and pelletized. The background correction was made using a reference of KBr pellets.

Raman Spectroscopy. Raman scattering measurements with the excitation laser lines of 488 and 785 nm were performed in a back-scattering geometry using a micro-Raman setup consisting of a spectrometer (model LabRAM HR, JobinYvon) and a Peltier-cooled charge-coupled device (CCD) detector. Raman spectra of all samples were recorded at room temperature in the frequency range of 100–4000 cm^{-1}.

Transmission Electron Microscopy (TEM). TEM images were taken using a FEI TecnaiTF-20 field-emission high-resolution transmission electron microscope operating at 200 kV. Samples for TEM imaging were prepared by placing a drop of as-prepared aqueous MoS_2@DNA solution on a carbon-coated Cu grid, and the solvent was evaporated under a light bulb.

Time-Correlated Single-Photon Counting. Picosecond-resolved fluorescence decay transients were measured using a commercially available spectrophotometer (Life Spec-ps, Edinburgh Instruments, U.K.) with 70 ps instrument response function (IRF). The observed fluorescence transients were fitted using a nonlinear least-squares fitting procedure to a function $[X(t) = \int_0^t E(t')R(t-t')dt']$ comprising of convolution of the IRF $[E(t)]$ with a sum of exponential $[R(t) = A + \sum_{i=1}^{N} B_i e^{-t/\tau_i}]$ with pre-exponential factors (B_i), characteristic lifetimes (τ_i), and a background (A). The relative concentration in a multi-exponential decay was finally expressed as $c_n = (B_n/\sum_{i=1}^{N} B_i) \times 100$. The quality of the curve fitting was evaluated by reduced χ^2 and residual data. It has to be noted that, with our time-resolved instrument, we can resolve at least one-fourth of the instrument response time constants after the deconvolution of the IRF.

RESULTS AND DISCUSSION

The process for synthesizing the MoS_2 NCs is simple and involves two steps (see the Experimental Section for details). First, the addition of molybdenum chloride to the DNA solution followed by the increase of pH to 9 (by the addition of NaOH) under vigorous stirring renders the molybdenum ion to be coordinated with the DNA. After 6–8 h, the solution becomes colorless. Finally, sodium sulfide (Na_2S) is added, and pH of the solution has been adjusted to 6 by adding HCl. The colorless solution turns yellow, indicating the formation of MoS_2 NCs. We have analyzed the as-synthesized NCs by various microscopic and spectroscopic techniques. A typical TEM image of the MoS_2 NCs is shown in Figure 1a. The NCs appear to be spherical in shape and fairly uniform in size. The particle sizes are estimated by fitting our experimental TEM data over 45 particles, which provides the mean diameter of ~5 nm (Figure 1b). High-resolution (HR) images of a single particle are shown in panels c and d of Figure 1. The HRTEM images shown in panels f and g of Figure 1 as well as the selected area electron diffraction (SAED) demonstrate the crystalline nature of the as-synthesized particles. The distance between two adjacent planes is 0.25 nm, corresponding to the (102) lattice plane of hexagonal MoS_2[37] [International Centre for Diffraction Data (ICDD), reference number 00-006-0097]. Further confirmation regarding the composition of as-prepared NCs is also evident from energy-dispersive X-ray spectroscopy (EDAX). A X-ray diffraction (XRD) study (see Figure S3 of the Supporting Information) confirms the presence of hexagonal MoS_2.

Figure 2a illustrates the UV–vis absorption spectra of DNA and MoS_2@DNA in water. Well-defined absorption bands featuring at 384 and 468 nm appear for the final MoS_2@DNA solution. Chikan et al. have reported a size-dependent spectroscopic study of MoS_2 nanoclusters.[28] They have established that MoS_2 nanoclusters having a size between 3 and 8 nm have absorption maxima around 362–470 nm.

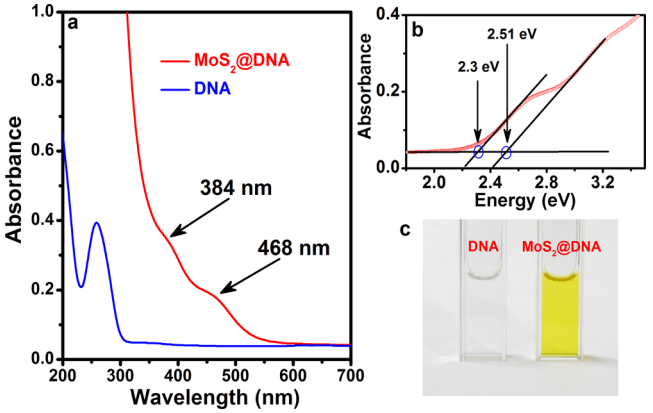

Figure 2. (a) UV–vis absorption spectra of DNA and MoS_2@DNA in water. Well-defined absorption bands of the NCs are marked with arrows. (b) Band gaps from the onset of the absorption bands of the MoS_2 NCs. (c) Photographs of DNA and MoS_2@DNA solutions under visible light.

dx.doi.org/10.1021/la4028578 | Langmuir 2013, 29, 11471–11478

Because the two absorption peaks are present in the MoS_2@DNA absorption spectrum, we associate the peaks with different sizes of MoS_2 NCs rather than first- and second-order quantum confined states of the same NCs. This observation is also consistent with the broad size distribution obtained from our TEM studies. The optical band gaps of MoS_2 NCs, measured from the onset of the absorption peaks, are ~2.30 and 2.51 eV, respectively (Figure 2b). Taking into account the band gap of bulk MoS_2, i.e., 1.29 eV, one might expect photoluminescence from the as-prepared NCs because of the large quantum confinement effect. However, no such photoluminescence has been observed from our as-prepared NCs (data not shown), which reveals that evolution of photoluminescence because of the quantum confinement effect may not be applicable for our NCs; rather, it is more relevant for MoS_2 nanosheets.[17] Photographs of the DNA and MoS_2@DNA solutions under visible light are shown in Figure 2c.

It is important to know the role of various parameters during the synthesis because it would be beneficial for scalable synthesis. We propose that sodium hydroxide has a role for the binding of the molybdenum ion to the DNA, whereas acidic medium assists the formation of hydrogen sulfide (H_2S) from Na_2S, which then reacts with the Mo−DNA complex. Direct addition of Na_2S to the molybdenum chloride solution at acidic pH leads to the formation of the bulk MoO_3 precipitate, as reflected from the Raman spectrum (see Figure S1 of the Supporting Information).[38] To investigate MoS_2 binding sites of DNA, we have performed FTIR studies. Figure 3 compares

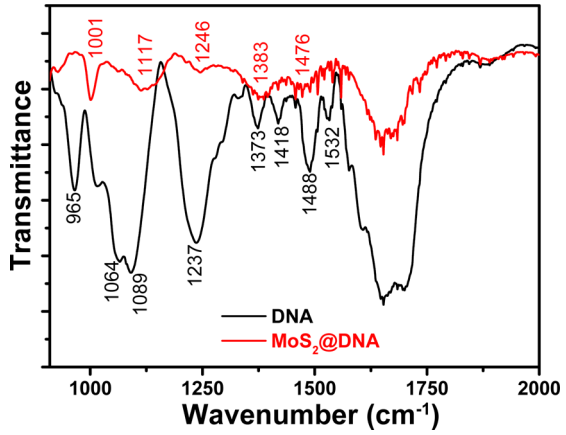

Figure 3. FTIR spectra of DNA (black color) and MoS_2@DNA (red color).

the FTIR of DNA and MoS_2@DNA. Absorptions in the 1500−1250 cm^{-1} region are caused by base-sugar vibrations. Sugar−phosphate vibrations appear in the 1250−1000 cm^{-1} region. From the spectra, we can observe that both of the spectral regions have perturbed significantly, which indicates that there is a significant interaction of MoS_2 with the DNA and that the samples are not merely mixtures of DNA and MoS_2.

Raman spectra have been recorded at ambient temperatures using different excitation wavelengths. Figure 4 displays the Raman spectra of MoS_2@DNA excited by 488 and 785 nm lines, respectively. It is clearly observed that there is a variation of peak intensity corresponding to the change in the excitation line. As depicted in Figure 4, the Raman spectra obtained upon excitation with the 488 nm line have peaks at 450 and 901 cm^{-1}, respectively, whereas a broad peak around 450 cm^{-1} has been observed for the 785 nm excitation line. The evident peak

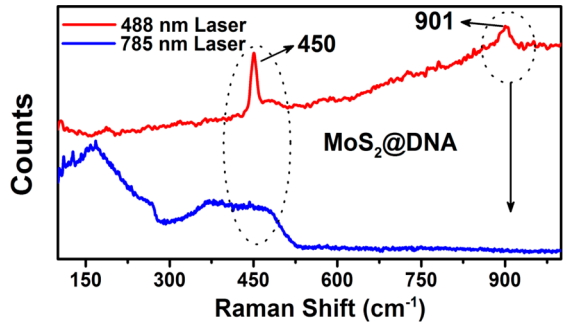

Figure 4. Raman characterization of MoS_2@DNA in the solid state using 488 nm (red) and 785 nm (blue) excitation lines.

broadening could be caused by the low spectral resolution of Raman spectroscopy with the 785 nm laser or because of the small size of the NCs integrated in large macromolecules. In contrast, in the case of 488 nm excitation, the Raman spectrum shows strong peaks, owing to the resonance Raman (RR) scattering, because the 488 nm line is in resonance with the band gap of the MoS_2 NCs (2.3 eV). Furthermore, the second-order Raman peak at 901 cm^{-1} also provides evidence about the RR effect.

Frey et al. disputed that the broad asymmetric peak around 450−460 cm^{-1} for bulk MoS_2 consists of two peaks, i.e., a second-order zone-edge phonon peak 2LA(M) at 454 cm^{-1} and a first-order optical phonon peak A_{2u} at 465 cm^{-1}.[39] Li et al. ascribed that the asymmetric feature splits into three peaks around 440, 450, and 459 cm^{-1}, where the 440 cm^{-1} peak has been assigned to Mo−S vibrations for oxysulfide species and the later provided the supportive evidence for the argument by Frey et al.[40] Most recently, Rao et al. have reported resonant Raman studies of a few layers of MoS_2, where they have found that the 450−460 cm^{-1} region becomes intense in resonance conditions.[41] Taking into account the high-resonance conditions, we anticipate that the 450 cm^{-1} peak observed for MoS_2 NCs excited by the 488 nm line is due to the strong electron−phonon coupling, as expected in RR scattering.

Because 2D MoS_2 has huge application in mechanics and field-effect transistors (FETs) at the nanoscale,[42−44] we choose to prepare a thin film of MoS_2 NCs. The procedure for the synthesis of the MoS_2@DNA−CTAC thin film has been mentioned in the Experimental Section. The UV−vis absorption spectrum of the film has been shown in the inset of Figure 5. Because both CTAC and DNA have no UV−vis absorption after 300 nm implies that 395 and 484 nm peaks are solely due to the MoS_2 NCs. Note that the absorption peaks have been red-shifted in the thin film, the effect of which is later reflected in the Raman spectrum of the MoS_2@DNA−CTAC thin film. In comparison to solid MoS_2@DNA, the MoS_2@DNA−CTAC thin film has more intense Raman peaks (excited by the 488 nm line), as depicted in Figure 5. Raman spectra of DNA and CTAC alone have also been shown in Figure 5. While most of the Raman peaks of DNA and CTAC remain unaltered, a strong peak at 447 cm^{-1} along with two other peaks at 896 and 1346 cm^{-1} are clearly evident in the MoS_2@DNA−CTAC thin film. The Raman peaks originating from the MoS_2 thin film are much stronger as well as blue-shifted about 3−4 cm^{-1} compared to MoS_2@DNA in the solid state. In obvious contrast, the strong resonance condition arises in the MoS_2 thin film, because the laser excitation energy coincides more with the electronic absorption band of the MoS_2 thin film

dx.doi.org/10.1021/la4028578 | Langmuir 2013, 29, 11471−11478

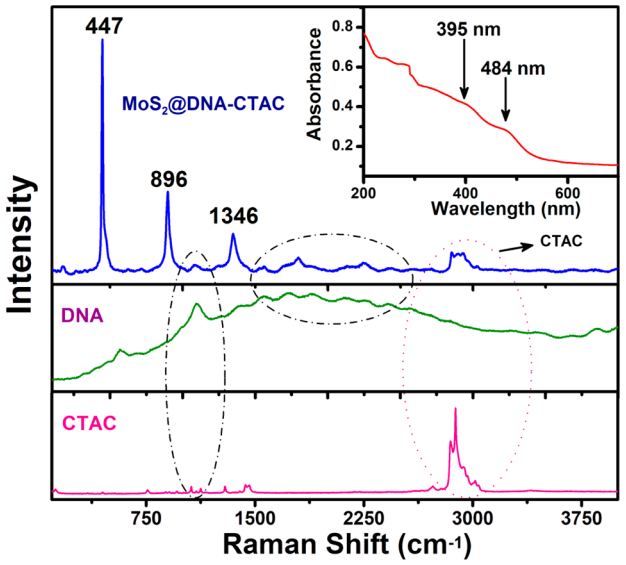

Figure 5. Raman spectra of CTAC (pink), DNA (green), and MoS_2@DNA−CTAC thin film (blue). The 488 nm excitation line has been used for the Raman studies. The inset shows the absorption spectrum of the MoS_2@DNA−CTAC thin film.

compared to MoS_2@DNA, causing an enhancement in the total scattering cross-section.

To investigate any conformational and structural changes in DNA as a result of the formation of MoS_2 NCs, Circular Dichroism (CD) spectroscopy has been carried out. Figure 6

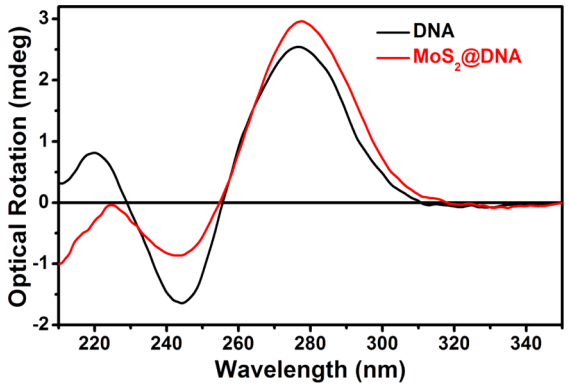

Figure 6. CD spectra of DNA and MoS_2@DNA in water.

represents the CD spectra of DNA, in the absence and presence of MoS_2 NCs. As evidenced from the figure, a negative band at 246 nm and a positive band at 280 nm point toward the B form of DNA, consistent with the existing literature.[45] Insignificant broadening with a slight red shift of the 280 nm band in the CD spectrum of MoS_2@DNA indicates a little perturbation of the DNA structure. A decrease of molar ellipticity of the 248 nm band as well as a slight increase of 280 nm band intensity in the presence of MoS_2 NCs indicate the perturbation of the overall secondary structure of the DNA. The study of the DNA−NP interaction by Narayanan et al. and many others has also reported this kind of perturbation and argued that the perturbation may be associated with the condensation of the DNA in the presence of NPs because it could easily wrap around the NPs as a result of its flexible nature.[46−48] Our study also provides supportive evidence for their argument.

A very recent studies by Rao et al. demonstrated that MoS_2 could be a p-type conductor; therefore, it would prefer to interact with electron donor molecules.[49] They have shown the charge-transfer interaction of MoS_2 with an electron donor molecule, such as tetrathiafulvalene (TTF), by monitoring the absorption band of TTF as well as MoS_2. We have also monitored the UV−vis spectrum of the MoS_2 NCs with various concentrations of a well-known electron donor; however, the absorption bands of MoS_2 NCs remain unaltered, indicating that MoS_2@DNA could not accept an electron in the ground state (see Figure S2 of the Supporting Information). It is widely accepted that nanomaterial confined in a biomolecule involves the energy transfer process, and several studies have been performed in this direction.[48,50,51] Now, the question is, could MoS_2 NCs adequately quench the fluorescence of the dye/donor molecules, so that it can replace some of the currently used nanomaterials? In the present study, we have taken H258 as a donor, which is a well-known dye that interacts with the minor grooves of the DNA molecule. Steady-state fluorescence measurements have been carried out on both the H258−DNA and MoS_2@H258−DNA solutions. It has been found that fluorescence of H258 underwent drastic quenching in the presence of MoS_2 NCs. Figure 7b depicts the fluorescence spectra of H258 without and with the presence of MoS_2 NCs. As evidenced from the figure, an unprecedented fluorescence quenching of 94% has been observed. The drastic quenching in the steady state obviously proves the efficacy of the MoS_2 NCs as a fluorescence quencher, however, does not provide any information about the nature of the quenching, i.e., whether it is static or dynamic. Picosecond-resolved fluorescence spectroscopy is a useful technique that provides information about the excited-state dynamics. Figure 7b shows the decay profiles of H258−DNA and MoS_2@H258−DNA monitored at the fluorescence maxima of the donor, i.e., at 470 nm (λ_{ex} = 375 nm). The decay transient of the donor (H258) has been fitted with two components, with an average lifetime of 2.6 ns. The fluorescence decay trace of the donor−acceptor (MoS_2@H258−DNA) could be fitted with a fast component, apparently corresponding to some non-radiative channel, along with two other components. The average lifetime of the donor−acceptor pair has been calculated to be 0.28 ns, which is much shorter than the average lifetime of the donor. Details of the fitting parameters of the time-resolved decays are tabulated in Table 1. Energy transfer, which involves deactivation of an electronic excited state of the donor and requires direct donor−acceptor spectral overlap, arises from the Columbic interaction between the donor and acceptor electric fields. Our study indeed demonstrates the incidence of a huge spectral overlap between the fluorescence of H258 (donor) and the absorbance of MoS_2 NCs (acceptor). The quenching of fluorescence decay transients and the spectral overlap, therefore, lead to the association of the energy transfer process.

The fitting result obtained from the decay transients is typical of a FRET donor decay transient, where rapid non-radiative transfer of energy from an excited donor to a ground-state acceptor manifests in a rapid drop off of the donor signal with time. We have estimated the energy transfer efficiency from the lifetime of the donor and donor−acceptor pair to be 89%. The energy transfer efficiency obtained from the lifetime measurements is different from the steady-state measurements, however, more reliable, because the former is more sensitive than the later as a result of the lamp fluctuation as well as many other processes. It is noteworthy to mention that we have

dx.doi.org/10.1021/la4028578 | Langmuir 2013, 29, 11471−11478

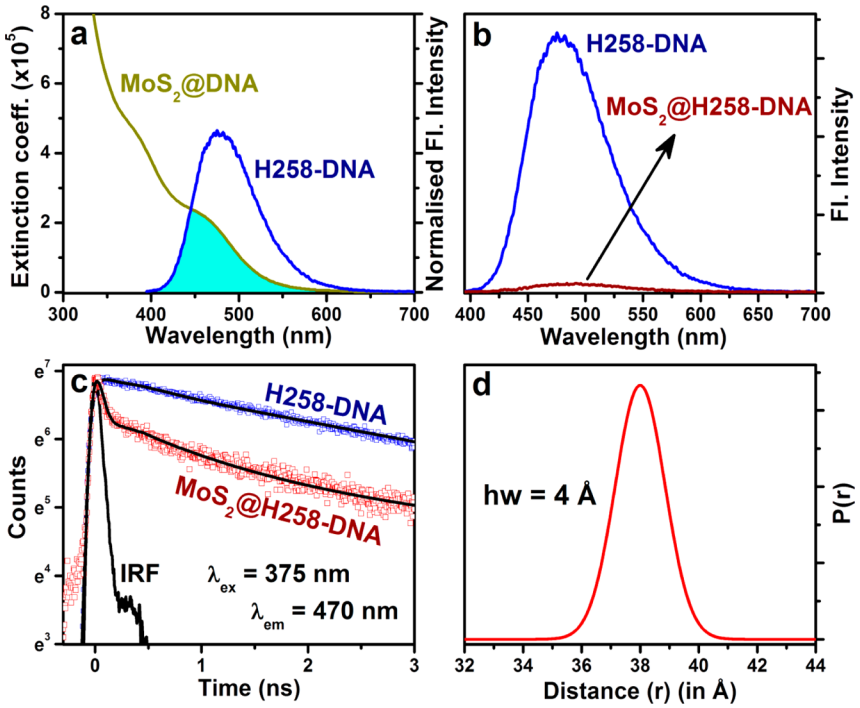

Figure 7. (a) Spectral overlap between the fluorescence spectrum of H258−DNA and the absorption spectrum of MoS_2@DNA (the extinction coefficient value is for the acceptor, MoS_2@DNA). (b) Steady-state fluorescence quenching of H258 in the presence of the acceptor MoS_2@DNA. (c) Picosecond-resolved fluorescence transients of H258−DNA and MoS_2@H258−DNA monitored at 470 nm (λ_{ex} = 375 nm). (d) Probability of the distance distribution $[P(r)]$ with respect to mean the donor−acceptor distance.

Table 1. Fitted Decay Time Constants of H258−DNA and MoS_2@H258−DNA from Picosecond-Resolved Experiments[a]

system	τ_1 (ns)	τ_2 (ns)	τ_3 (ns)	τ_{av} (ns)
H258−DNA	0.30 (25%)	3.40 (75%)	0.00	2.60
MoS_2@H258−DNA	0.02 (90%)	0.92 (6%)	6.1 (4%)	0.28

[a]Values in parentheses represent the relative weight percentage of the time components. The standard error is ∼5%.

calculated the donor−acceptor distance using the FRET method. Details of FRET have been described in the Experimental Section (see the Supporting Information). We have estimated the overlap integral $J(\lambda)$ to be 6.86×10^{15} M^{-1} cm^{-1} nm^4 according to eq 2 (see the Supporting Information). The characteristic Förster distance (R_0) is calculated to be 55 Å. Using the efficiency of FRET, we have calculated the donor−acceptor distance (r) to be 38 Å. Taking into account that the average radius of the MoS_2 NC is 2.5 nm (25 Å) (from the TEM measurements), the calculated donor−acceptor distance indicates that the residing probability of the donor H258 is very close to the surface of the NCs. To obtain an idea of the probability distribution of the donor−acceptor distance, we have analyzed the time-resolved decay transients of H258 in the presence and absence of MoS_2 NCs to construct the distance distribution function, $P(r)$ (see the Experimental Section for details). As evident in Figure 7d, the half width (hw) of the distance distribution is found to be 4 Å. This corresponds to a very high efficiency of energy transfer.

For a better understanding of the energy transfer between the excited state of H258 with MoS_2 NCs, it is essential to know the distribution of the acceptor (MoS_2 NCs) around the H258 molecules (bonded to the minor groove of DNA), because this is a governing factor that can influence the efficient energy transfer, as observed from the time-resolved fluorescence studies (Figure 7c). In this regard, we have applied a kinetic model developed by Tachiya for the quenching of fluorescent probes.[35,36] Figure 8 demonstrates the time-resolved fluorescence transients of H258 in the absence and presence of MoS_2 NCs, and black curves correspond to the fitting of the decay transients with eqs 15 and 16 (see the Experimental Section of the Supporting Information for details). The observed fluorescence transients were fitted using a nonlinear least-squares fitting procedure (software SCIENTIST) to a function $[X(t) = \int_0^t E(t')P(t - t')dt']$ comprising of the convolution of the instrument response

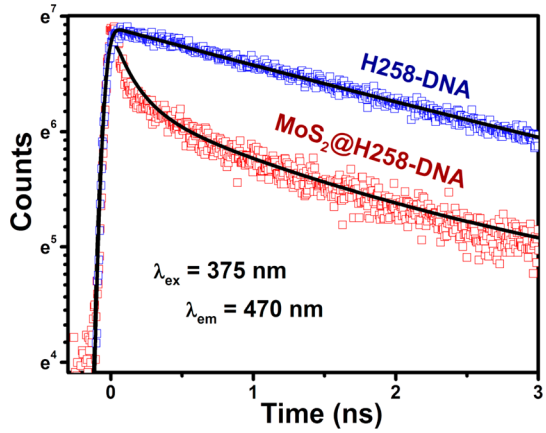

Figure 8. Picosecond-resolved fluorescence transients of H258−DNA (blue) and MoS_2@H258−DNA (red), fitted with the kinetic model by Tachiya. The fitted curves are shown in black.

dx.doi.org/10.1021/la4028578 | Langmuir 2013, 29, 11471−11478

function (IRF) $[E(t)]$ with the exponential $(p(t,m) = P(0)\exp\{-k_0t - m_t[1 - \exp(-k_{qt}t)] - m[1 - \exp(-k_qt)]\})$. The purpose of this fitting is to obtain the decays in an analytic form suitable for further data analysis. Reasonably good fitting has been observed from the model. The quenching parameters are summarized in Table 2. The quenching rate constant (k_{qt}), which corresponds to unidentified traps, is same even after the addition of the acceptor (MoS_2 NCs), and this indicates the average number of unidentified trap states to be the same. However, it is observed from Table 2 that the average number of unidentified trap states (m) increases with the addition of acceptor molecules. Because there are still many unknown parameters in the excitation dynamics of H258, for an accurate interpretation of this observation, a more complex model is required. One important finding is that the mean number of acceptors (MoS_2 NCs) associated with each donor is 1.08, and the estimated rate constant for energy transfer (k_q) per acceptor molecules is 6 ns^{-1}. The energy transfer rate calculated from the conventional FRET model has been found to be comparable (3.57 ns^{-1}) to the value obtained using the model by Tachiya (6 ns^{-1}).

Table 2. Overview of the Value of Quenching Parameters Using the Kinetic Model Developed by Tachiya[a]

system	k_o (ns^{-1})	m_t	k_{qt} (ns^{-1})	m	k_q (ns^{-1})
H258−DNA	0.01	8.47	0.03		
MoS_2@H258−DNA	0.01	8.47	0.03	1.08	6

[a] k_o is the total decay constant of H258 in the excited state in the absence of the acceptor NCs. m_t is the average number of unidentified traps around the donor H258 following a Poisson distribution. k_{qt} quenching rate constant by unidentified traps. m is the mean number of H258−DNA molecules attached to one NC. k_q is the rate constant for energy transfer for one H258−DNA molecule.

CONCLUSION

In conclusion, well-crystallized ∼5 nm MoS_2 NCs have been synthesized in the DNA matrix. The calculated band gaps from the optical absorption of MoS_2 NCs confirm the quantum confinement of the NCs conjugated with the DNA matrix. A strong electron−phonon resonance condition makes MoS_2 NCs Raman-active. In comparison to MoS_2 NCs, the MoS_2 thin film has more intense Raman peaks because the laser excitation energy coincides more with the electronic absorption band of the MoS_2@DNA−CTAC thin film compared to MoS_2@DNA. Moreover, the present study also reveals that, similar to the other various nanomaterials, MoS_2 NCs would have a profound impact as an efficient fluorescence quencher. Analysis suggests that the fluorescence quenching of the donor in the presence of MoS_2 NCs is mainly due to a non-radiative decay channel, which confirms the energy transfer process. The donor−acceptor distance of 38 Å has been estimated using the efficiency of the FRET model. Further analysis of the probability of the donor−acceptor distance distribution suggests that the donor molecules are very close in proximity to the surface of the NCs. We have employed a kinetic model developed by Tachiya to understand the kinetics of energy transfer from H258 to MoS_2 NCs, assuming that the Poisson distribution of the quencher molecules around H258 bonded to the DNA minor grooves, which closely resembles the FRET data. Such a synthetic route of MoS_2 NCs as well as a thin film based on the DNA template may be extended to the other transition-metal chalcogenide materials, and we believe that MoS_2 NC-based energy transfer is expected to grow in the near future.

ASSOCIATED CONTENT

Supporting Information

Detailed experimental procedures, Raman spectra of MoO_3, and XRD of MoS_2@DNA. This material is available free of charge via the Internet at http://pubs.acs.org.

AUTHOR INFORMATION

Corresponding Author

*E-mail: skpal@bose.res.in.

Notes

The authors declare no competing financial interest.

ACKNOWLEDGMENTS

Nirmal Goswami thanks CSIR, India, for fellowship. Anupam Giri thanks UGC, India, for fellowship. The authors thank Dr. Achintya Singha for his assistance in Raman experiments, Samik Roy Moulik for his assistance in TEM experiments, and the Department of Science and Technology (DST), Government of India, for financial grants (DST/TM/SERI/2k11/103).

REFERENCES

(1) Medintz, I. L.; Stewart, M. H.; Trammell, S. A.; Susumu, K.; Delehanty, J. B.; Mei, B. C.; Melinger, J. S.; Blanco-Canosa, J. B.; Dawson, P. E.; Mattoussi, H. Quantum-dot/dopamine bioconjugates function as redox coupled assemblies for in vitro and intracellular pH sensing. *Nat. Mater.* **2010**, *9* (8), 676−684.

(2) Goswami, N.; Giri, A.; Kar, S.; Bootharaju, M. S.; John, R.; Xavier, P. L.; Pradeep, T.; Pal, S. K. Protein-directed synthesis of NIR-emitting, tunable HgS quantum dots and their applications in metal-ion sensing. *Small* **2012**, *8* (20), 3175−3184.

(3) Wang, Q. H.; Kalantar-Zadeh, K.; Kis, A.; Coleman, J. N.; Strano, M. S. Electronics and optoelectronics of two-dimensional transition metal dichalcogenides. *Nat. Nanotechnol.* **2012**, *7* (11), 699−712.

(4) Xiang, Q.; Yu, J.; Jaroniec, M. Synergetic effect of MoS_2 and graphene as cocatalysts for enhanced photocatalytic H_2 production activity of TiO_2 nanoparticles. *J. Am. Chem. Soc.* **2012**, *134* (15), 6575−6578.

(5) Ho, W.; Yu, J. C.; Lin, J.; Yu, J.; Li, P. Preparation and photocatalytic behavior of MoS_2 and WS_2 nanocluster sensitized TiO_2. *Langmuir* **2004**, *20* (14), 5865−5869.

(6) Radisavljevic, B.; Radenovic, A.; Brivio, J.; Giacometti, V.; Kis, A. Single-layer MoS_2 transistors. *Nat. Nanotechnol.* **2011**, *6* (3), 147−150.

(7) Shen, R.; Shen, X.; Zhang, Z.; Li, Y.; Liu, S.; Liu, H. Multifunctional conjugates to prepare nucleolar-targeting CdS quantum dots. *J. Am. Chem. Soc.* **2010**, *132* (25), 8627−8634.

(8) Michalet, X.; Pinaud, F. F.; Bentolila, L. A.; Tsay, J. M.; Doose, S.; Li, J. J.; Sundaresan, G.; Wu, A. M.; Gambhir, S. S.; S., W. Quantum dots for live cells, in vivo imaging, and diagnostics. *Science* **2005**, *307* (5709), 538−544.

(9) Mak, K. F.; Lee, C.; Hone, J.; Shan, J.; Heinz, T. F. Atomically thin MoS_2: A new direct-gap semiconductor. *Phys. Rev. Lett.* **2010**, *105* (13), 136805.

(10) Liu, K.-K.; Zhang, W.; Lee, Y.-H.; Lin, Y.-C.; Chang, M.-T.; Su, C.-Y.; Chang, C.-S.; Li, H.; Shi, Y.; Zhang, H.; Lai, C.-S.; Li, L.-J. Growth of large-area and highly crystalline MoS_2 thin layers on insulating substrates. *Nano Lett.* **2012**, *12* (3), 1538−1544.

(11) Chang, L.; Yang, H.; Fu, W.; Zhang, J.; Yu, Q.; Zhu, H.; Chen, J.; Wei, R.; Sui, Y.; Pang, X.; Zou, G. Simple synthesis of MoS_2 inorganic fullerene-like nanomaterials from MoS_2 amorphous nanoparticles. *Mater. Res. Bull.* **2008**, *43* (8−9), 2427−2433.

(12) Nath, M.; Govindaraj, A.; Rao, C. N. R. Simple synthesis of MoS_2 and WS_2 nanotubes. *Adv. Mater.* **2001**, *13* (4), 283−286.

(13) Yu, H.; Liu, Y.; Brock, S. L. Synthesis of discrete and dispersible MoS_2 nanocrystals. *Inorg. Chem.* **2008**, *47* (5), 1428−1434.
(14) Liao, H.; Wang, Y.; Zhang, S.; Qian, Y. A solution low-temperature route to MoS_2 fiber. *Chem. Mater.* **2000**, *13* (1), 6−8.
(15) Ataca, C.; Şahin, H.; Aktürk, E.; Ciraci, S. Mechanical and electronic properties of MoS_2 nanoribbons and their defects. *J. Phys. Chem. C* **2011**, *115* (10), 3934−3941.
(16) Late, D. J.; Liu, B.; Matte, H. S. S. R.; Dravid, V. P.; Rao, C. N. R. Hysteresis in single-layer MoS_2 field effect transistors. *ACS Nano* **2012**, *6* (6), 5635−5641.
(17) Splendiani, A.; Sun, L.; Zhang, Y.; Li, T.; Kim, J.; Chim, C.-Y.; Galli, G.; Wang, F. Emerging photoluminescence in monolayer MoS_2. *Nano Lett.* **2010**, *10* (4), 1271−1275.
(18) Afanasiev, P.; Geantet, C.; Llorens, I.; Proux, O. Biotemplated synthesis of highly divided MoS_2 catalysts. *J. Mater. Chem.* **2012**, *22* (19), 9731−9737.
(19) O'Neill, A.; Khan, U.; Coleman, J. N. Preparation of high concentration dispersions of exfoliated MoS_2 with increased flake size. *Chem. Mater.* **2012**, *24* (12), 2414−2421.
(20) Lee, Y.-H.; Zhang, X.-Q.; Zhang, W.; Chang, M.-T.; Lin, C.-T.; Chang, K.-D.; Yu, Y.-C.; Wang, J. T.-W.; Chang, C.-S.; Li, L.-J.; Lin, T.-W. Synthesis of large-area MoS_2 atomic layers with chemical vapor deposition. *Adv. Mater.* **2012**, *24* (17), 2320−2325.
(21) Nagaraju, G.; Tharamani, C. N.; Chandrappa, G. T.; Livage, J. Hydrothermal synthesis of amorphous MoS_2 nanofiber bundles via acidification of ammonium heptamolybdate tetrahydrate. *Nanoscale Res. Lett.* **2007**, *2* (9), 461−468.
(22) Liu, S.; Zhang, X.; Shao, H.; Xu, J.; Chen, F.; Feng, Y. Preparation of MoS_2 nanofibers by electrospinning. *Mater. Lett.* **2012**, *73* (0), 223−225.
(23) Ramakrishna Matte, H. S. S.; Gomathi, A.; Manna, A. K.; Late, D. J.; Datta, R.; Pati, S. K.; Rao, C. N. R. MoS_2 and WS_2 analogues of graphene. *Angew. Chem., Int. Ed.* **2010**, *49* (24), 4059−4062.
(24) Etzkorn, J.; Therese, H. A.; Rocker, F.; Zink, N.; Kolb, U.; Tremel, W. Metal−organic chemical vapor depostion synthesis of hollow inorganic-fullerene-type MoS_2 and $MoSe_2$ nanoparticles. *Adv. Mater.* **2005**, *17* (19), 2372−2375.
(25) Li, X.-L.; Ge, J.-P.; Li, Y.-D. Atmospheric pressure chemical vapor deposition: An alternative route to large-scale MoS_2 and WS_2 inorganic fullerene-like nanostructures and nanoflowers. *Chem.—Eur. J.* **2004**, *10* (23), 6163−6171.
(26) Uzcanga, I.; Bezverkhyy, I.; Afanasiev, P.; Scott, C.; Vrinat, M. Sonochemical preparation of MoS_2 in aqueous solution: Replication of the cavitation bubbles in an inorganic material morphology. *Chem. Mater.* **2005**, *17* (14), 3575−3577.
(27) Peng, Y.; Meng, Z.; Zhong, C.; Lu, J.; Yu, W.; Yang, Z.; Qian, Y. Hydrothermal synthesis of MoS_2 and its pressure-related crystallization. *J. Solid State Chem.* **2001**, *159* (1), 170−173.
(28) Chikan, V.; Kelley, D. F. Size-dependent spectroscopy of MoS_2 nanoclusters. *J. Phys. Chem. B* **2002**, *106* (15), 3794−3804.
(29) Zhou, W.; Baneyx, F. Aqueous, protein-driven synthesis of transition metal-doped ZnS immuno-quantum dots. *ACS Nano* **2011**, *5* (10), 8013−8018.
(30) Medintz, I. L.; Uyeda, H. T.; Goldman, E. R.; Mattoussi, H. Quantum dot bioconjugates for imaging, labelling and sensing. *Nat. Mater.* **2005**, *4* (6), 435−446.
(31) Levina, L.; Sukhovatkin, V.; Musikhin, S.; Cauchi, S.; Nisman, R.; Bazett-Jones, D. P.; Sargent, E. H. Efficient infrared-emitting PbS quantum dots grown on DNA and stable in aqueous solution and blood plasma. *Adv. Mater.* **2005**, *17* (15), 1854−1857.
(32) Narayanan, S. S.; Sarkar, R.; Pal, S. K. Structural and functional characterization of enzyme−quantum dot conjugates: Covalent attachment of CdS nanocrystal to α-chymotrypsin. *J. Phys. Chem. C* **2007**, *111* (31), 11539−11543.
(33) Jones, M. R.; Macfarlane, R. J.; Lee, B.; Zhang, J.; Young, K. L.; Senesi, A. J.; Mirkin, C. A. DNA−nanoparticle superlattices formed from anisotropic building blocks. *Nat. Mater.* **2010**, *9* (11), 913−917.
(34) Aldaye, F. A.; Sleiman, H. F. Dynamic DNA templates for discrete gold nanoparticle assemblies: Control of geometry, modularity, write/erase and structural switching. *J. Am. Chem. Soc.* **2007**, *129* (14), 4130−4131.
(35) Tachiya, M. Application of a generating function to reaction kinetics in micelles. Kinetics of quenching of luminescent probes in micelles. *Chem. Phys. Lett.* **1975**, *33* (2), 289−292.
(36) Tachiya, M. Kinetics of quenching of luminescent probes in micellar systems. II. *J. Chem. Phys.* **1982**, *76* (1), 340−348.
(37) Albiter, M. A.; Huirache-Acuna, R.; Paraguay-Delgado, F.; Rico, J. L.; Alonso-Nunez, G. Synthesis of MoS_2 nanorods and their catalytic test in the HDS of dibenzothiophene. *Nanotechnology* **2006**, *17* (14), 3473−3481.
(38) Windom, B.; Sawyer, W. G.; Hahn, D. A Raman spectroscopic study of MoS_2 and MoO_3: Applications to tribological systems. *Tribol. Lett.* **2011**, *42* (3), 301−310.
(39) Frey, G. L.; Tenne, R.; Matthews, M. J.; Dresselhaus, M. S.; Dresselhaus, G. Raman and resonance Raman investigation of MoS_2 nanoparticles. *Phys. Rev. B: Condens. Matter Mater. Phys.* **1999**, *60* (4), 2883−2892.
(40) Li, H.; Zhang, Q.; Yap, C. C. R.; Tay, B. K.; Edwin, T. H. T.; Olivier, A.; Baillargeat, D. From bulk to monolayer MoS_2: Evolution of Raman scattering. *Adv. Funct. Mat.* **2012**, *22* (7), 1385−1390.
(41) Chakraborty, B.; Matte, H. S. S. R.; Sood, A. K.; Rao, C. N. R. Layer-dependent resonant Raman scattering of a few layer MoS_2. *J. Raman Spectrosc.* **2013**, *44* (1), 92−96.
(42) Hwang, W. S.; Remskar, M.; Yan, R. S.; Kosel, T.; Park, J. K.; Cho, B. J.; Haensch, W.; Xing, H. L.; Seabaugh, A.; Jena, D. Comparative study of chemically synthesized and exfoliated multilayer MoS_2 field-effect transistors. *Appl. Phys. Lett.* **2013**, *102* (4), 043116.
(43) Min, S.-W.; Lee, H. S.; Choi, H. J.; Park, M. K.; Nam, T.; Kim, H.; Ryu, S.; Im, S. Nanosheet thickness-modulated MoS_2 dielectric property evidenced by field-effect transistor performance. *Nanoscale* **2013**, *5* (2), 548−551.
(44) Castellanos-Gomez, A.; Poot, M.; Steele, G. A.; van der Zant, H. S. J.; Agraït, N.; Rubio-Bollinger, G. Elastic properties of freely suspended MoS_2 nanosheets. *Adv. Mater.* **2012**, *24* (6), 772−775.
(45) Sarkar, R.; Pal, S. K. Ligand−DNA interaction in a nanocage of reverse micelle. *Biopolymers* **2006**, *83* (6), 675−686.
(46) Shankara Narayanan, S.; Sinha, S. S.; Verma, P. K.; Pal, S. K. Ultrafast energy transfer from 3-mercaptopropionic acid-capped CdSe/ZnS QDs to dye-labelled DNA. *Chem. Phys. Lett.* **2008**, *463* (1−3), 160−165.
(47) Jin, R.; Wu, G.; Li, Z.; Mirkin, C. A.; Schatz, G. C. What controls the melting properties of DNA-linked gold nanoparticle assemblies? *J. Am. Chem. Soc.* **2003**, *125* (6), 1643−1654.
(48) Giri, A.; Goswami, N.; Lemmens, P.; Pal, S. K. Preparation of water soluble L-arginine capped CdSe/ZnS QDs and their interaction with synthetic DNA: Picosecond-resolved FRET study. *Mater. Res. Bull.* **2012**, *47* (8), 1912−1918.
(49) Dey, S.; Matte, H. S. S. R.; Shirodkar, S. N.; Waghmare, U. V.; Rao, C. N. R. Charge-transfer interaction between few-layer MoS_2 and tetrathiafulvalene. *Chem.—Asian J.* **2013**, *8* (8), 1780−1784.
(50) Sen, T.; Patra, A. Recent advances in energy transfer processes in gold-nanoparticle-based assemblies. *J. Phys. Chem. C* **2012**, *116* (33), 17307−17317.
(51) Medintz, I. L.; Pons, T.; Susumu, K.; Boeneman, K.; Dennis, A. M.; Farrell, D.; Deschamps, J. R.; Melinger, J. S.; Bao, G.; Mattoussi, H. Resonance energy transfer between luminescent quantum dots and diverse fluorescent protein acceptors. *J. Phys. Chem. C* **2009**, *113* (43), 18552−18561.